Article

Cell Reports

Roles for Cell-Cell Adhesion and Contact in Obesity-Induced Hepatic Myeloid Cell Accumulation and Glucose Intolerance

Graphical Abstract

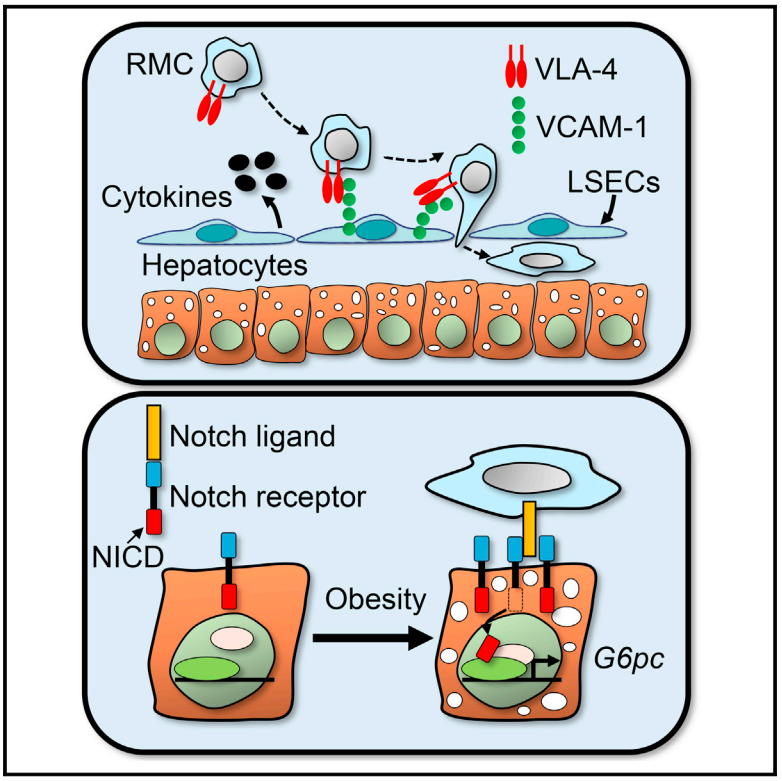

Highlights

- Obesity enhances VLA-4-dependent cell-cell adhesion between LSEC and myeloid cells
- VLA-4 blockade improves hyperglycemia in obese mice
- Cell-cell contact between leukocytes and hepatocytes promotes gluconeogenesis

Authors

Yasutaka Miyachi, Kyoichiro Tsuchiya, Chikara Komiya, ..., Masayuki Yoshida, Masaru Ishii, Yoshihiro Ogawa

Correspondence

ktsuchiya.mem@tmd.ac.jp (K.T.), ogawa.mem@tmd.ac.jp (Y.O.)

In Brief

Obesity promotes myeloid cell accumulation in the liver, increasing hepatic inflammation and glucose intolerance. Miyachi et al. find that liver sinusoidal endothelial cells play an important role in hepatic myeloid cell accumulation via VLA-4-dependent cell-cell adhesion. Accumulating myeloid cells activate Notch signaling and gluconeogenesis in hepatocytes through cell-cell contact.

Accession Numbers

GSE84019
GSE85673

Miyachi et al., 2017, Cell Reports *18*, 2766–2779
March 14, 2017
http://dx.doi.org/10.1016/j.celrep.2017.02.039

OPEN ACCESS
CellPress

Cell Reports
Article

Roles for Cell-Cell Adhesion and Contact in Obesity-Induced Hepatic Myeloid Cell Accumulation and Glucose Intolerance

Yasutaka Miyachi,[1] Kyoichiro Tsuchiya,[1,*] Chikara Komiya,[1] Kumiko Shiba,[1] Noriko Shimazu,[1] Shinobu Yamaguchi,[1] Michiyo Deushi,[2] Mizuko Osaka,[2] Kouji Inoue,[3] Yuta Sato,[4] Sayaka Matsumoto,[4] Junichi Kikuta,[4] Kenjiro Wake,[3] Masayuki Yoshida,[2] Masaru Ishii,[4] and Yoshihiro Ogawa[1,5,6,7,*]

[1]Department of Molecular Endocrinology and Metabolism
[2]Department of Life Science and Bioethics
Graduate School of Medical and Dental Sciences, Tokyo Medical and Dental University, Bunkyo-ku, Tokyo 113-8510, Japan
[3]Department of Anatomy and Histocytology, School of Dental Medicine, Tsurumi University, Yokohama, Kanagawa 230-8501, Japan
[4]Department of Immunology and Cell Biology, Graduate School of Medicine and Frontier Biosciences, Osaka University, Suita, Osaka 565-0871, Japan
[5]Department of Medicine and Bioregulatory Science, Graduate School of Medical Sciences, Kyushu University, Fukuoka, Fukuoka 812-8582, Japan
[6]Japan Agency for Medical Research and Development, CREST, Chiyoda-ku, Tokyo 100-0004, Japan
[7]Lead Contact
*Correspondence: ktsuchiya.mem@tmd.ac.jp (K.T.), ogawa.mem@tmd.ac.jp (Y.O.)
http://dx.doi.org/10.1016/j.celrep.2017.02.039

SUMMARY

Obesity promotes infiltration of inflammatory cells into various tissues, leading to parenchymal and stromal cell interaction and development of cellular and organ dysfunction. Liver sinusoidal endothelial cells (LSECs) are the first cells that contact portal blood cells and substances in the liver, but their functions in the development of obesity-associated glucose metabolism remain unclear. Here, we find that LSECs are involved in obesity-associated accumulation of myeloid cells via VLA-4-dependent cell-cell adhesion. VLA-4 blockade in mice fed a high-fat diet attenuated myeloid cell accumulation in the liver to improve hepatic inflammation and systemic glucose intolerance. Ex vivo studies further show that cell-cell contact between intrahepatic leukocytes and parenchymal hepatocytes induces gluconeogenesis via a Notch-dependent pathway. These findings suggest that cell-cell interaction between parenchymal and stromal cells regulates hepatic glucose metabolism and offers potential strategies for treatment or prevention of obesity-associated glucose intolerance.

INTRODUCTION

The liver is a major site of endogenous glucose production. Hepatic insulin resistance involves inadequate insulin-mediated suppression of hepatic glucose output, which has a critical role in the pathogenesis of glucose intolerance. In recent years, chronic inflammation has been identified as a major contributor to decreased insulin sensitivity in obesity and plays a role in the pathogenesis of obesity-associated hepatic and systemic glucose intolerance (Olefsky and Glass, 2010; Osborn and Olefsky, 2012). Obesity promotes hepatic inflammation in humans and rodents, which is associated with increased production of inflammatory cytokines and substances that impair hepatic insulin sensitivity (Oh et al., 2012; Olefsky and Glass, 2010; Osborn and Olefsky, 2012; Talukdar et al., 2012). At the cellular level, there is evidence that infiltration of inflammatory cells into the liver promotes hepatic inflammation. Studies have described that obesity promotes liver infiltration of recruited myeloid cells (RMCs) (Morinaga et al., 2015; Obstfeld et al., 2010; Oh et al., 2012; Talukdar et al., 2012), which are a distinct population from resident Kupffer cells. RMCs express C-C chemokine receptor type 2 (CCR-2) and are recruited to the liver through the monocyte chemotactic protein-1 (MCP-1) in a CCR-2-dependent manner (Obstfeld et al., 2010). In addition, RMCs in obese mice have been shown to exacerbate insulin resistance and hepatic inflammation (Cai et al., 2005; Jia et al., 2014). RMC accumulation thus promotes obesity-induced hepatic and systemic glucose intolerance.

For recruitment and infiltration of inflammatory cells into parenchymal organs, endothelial cells generally play a pivotal role in adhesion molecule-mediated cell trafficking and transmigration. In the liver, sinusoids are lined by a unique population of liver sinusoidal endothelial cells (LSECs), which comprise one of the first hepatic cell populations that comes into contact with blood components. They possess no tight junctions without basement membrane, being separated from underlying hepatocytes only by the space of Disse. Similar to typical vascular endothelial cells, adhesion molecules, such as intercellular adhesion molecule-1 (ICAM-1), vascular cell adhesion molecule-1 (VCAM-1), and E- and P-selectins, are expressed in LSECs and bind to their respective ligands, such as lymphocyte function-associated antigen-1 (LFA-1), very late antigen-4 (VLA-4), E-selectin ligand-1 (ESL-1), and P-selectin glycoprotein ligand-1 (PSGL-1), on leukocytes. Therefore, it is conceivable that during obesity-induced RMC accumulation in the liver,

LSECs interact with RMCs in the sinusoid by production of cytokines or chemokines and cell-cell adhesion. Furthermore, once infiltrated into the liver, RMCs may make direct contact with parenchymal hepatocytes, thereby affecting hepatic metabolism. However, it is unclear whether physical cell-cell interaction among RMCs, LSECs, and hepatocytes modulates hepatic inflammation and metabolic function.

In this paper, we aimed to examine the role of LSECs in obesity-induced glucose intolerance via VLA-4-mediated cell adhesion and hepatic accumulation of RMCs. Our data suggest that infiltrating RMCs can increase glucose production in neighboring hepatocytes through activation of the Notch signaling pathway, which is induced by cell-cell contact. Collectively, we postulate a mechanism in which hepatic glucose metabolism is regulated through parenchymal-stromal cell interaction, thus offering potential strategies to treat or prevent obesity-associated glucose intolerance.

RESULTS

Obesity Increases RMC Accumulation in the Liver, along with Upregulation of Cell Adhesion Molecules

We first interrogated changes in gene expression of cell adhesion molecules in the liver during high-fat diet (HFD) feeding. During a 4-week HFD feeding, wild-type (WT) mice gained weight and developed adiposity (Figures 1A and S1A). Fasting hyperglycemia and hyperinsulinemia, hepatic steatosis, and liver injury, as assessed by serum alanine aminotransferase (ALT) levels, were observed at 10 weeks of HFD feeding and thereafter (Figure 1A). Along with deterioration of metabolic profiles, there was upregulation of the genes of cell adhesion molecules (*Icam1*, *Vcam1*, *Sele*, and *Selp*) and their cognate ligands (*Itgal*, *Itga4*, *Esl1*, and *Selplg*) by HFD feeding (Figure 1B). Eight-week-old genetically obese *ob*/*ob* mice also showed liver induction compared with the WT mice. In both HFD-fed and *ob*/*ob* mice, gene induction was partially reversed by treatment with a sodium-glucose co-transporter 2 inhibitor, ipragliflozin, for 4 weeks (Figure S1B). In addition, genes of *Vcam1* and *Sele* were upregulated in the liver of patients with type 2 diabetes, compared with control subjects (Figure 1C).

Using flow cytometry analysis (Figure S2A), we next examined changes in RMC accumulation in the liver during HFD feeding. Backgating analysis of flow cytometry data showed that >80% of the RMCs were monocytes and neutrophils, both of which were mostly included in the RMC population on the mice fed a standard diet (SD) and those fed an HFD (Figures S2B–S2D). In parallel with the progression of impaired glucose and lipid metabolism, RMCs, monocytes, and neutrophils were observed to accumulate in the liver during 16 weeks of HFD feeding (Figures 2A, 2B, and S2E). Histologic analysis showed increased numbers of intrahepatic CCR-2-positive (RMC marker) and Gr-1-positive (neutrophil marker) cells in response to the HFD feeding (Figure 2C). Toluidine blue staining revealed that in HFD-fed mice, more mononuclear cells were infiltrated into the perisinusoidal space, where mononuclear cells appeared to be in direct contact with the neighboring hepatocytes (Figure 2D). On electron microscopy analysis, HFD did not affect the microstructure of sinusoidal walls, but the activated monocytes that were adherent to the sinusoidal walls and the infiltrated macrophages among hepatocytes were frequently observed in the liver of HFD-fed mice, compared with SD-fed mice (Figure 2E). We observed similar findings in the liver of *ob*/*ob* mice (Figure S2F). These observations suggested that obesity upregulated cell adhesion molecules and increased RMC accumulation in the liver, along with metabolic deterioration. Furthermore, our data revealed that RMCs were localized in sinusoidal walls and among the hepatocytes during development of obesity.

Obesity Promotes Myeloid Cell Adhesion to LSECs

We hypothesized that increased cell adhesion with the sinusoidal wall caused RMCs to accumulate in the liver. To assess the dynamic behavior of myeloid cells, we carried out intravital imaging in the liver from lysozyme M-EGFP transgenic (*LysM*^{EGFP}) mice, whose EGFP was specifically expressed in the myeloid lineage (Faust et al., 2000). Flow cytometry confirmed EGFP expression in RMCs, monocytes, and neutrophils (data not shown). The number of rolling and adherent *LysM*-positive cells significantly increased in *LysM*^{EGFP} mice with the *ob*/*ob* background, compared with those with the WT background (Figures 3A and 3B; Movies S1 and S2). Consistently, quantification of the imaging data showed that cell tracking velocity was significantly decreased in *LysM*^{EGFP} mice with the *ob*/*ob* background compared with those with the WT background (Figure 3C).

To explore whether cell-cell adhesion between LSECs and RMCs was enhanced in obesity, we examined LSECs isolated by magnetic beads that were conjugated by anti-CD146 antibodies. Pathway analysis of microarray data revealed upregulation of genes related to cell adhesion, the chemokine signaling pathway, and leukocyte transendothelial migration in LSECs in *ob*/*ob* mice, compared with WT mice (Figure S3A). qRT-PCR analysis confirmed that the genes of adhesion molecules (*Icam1*, *Vcam1*, *Sele*, and *Selp*) were upregulated in isolated LSECs of HFD-fed mice, compared with those of SD-fed mice (Figure 4A). Flow cytometry confirmed the increase of VCAM-1 protein expression in LSECs from HFD-fed mice compared with that from SD-fed mice. (Figures 4B and S3B). In addition, the genes of *Ccl2* and *Il6* significantly increased in the LSECs of HFD-fed mice (Figure 4A). Although Kupffer cells have been reported to strongly express *Ccl2* gene compared with RMCs (Morinaga et al., 2015), LSECs accounted for a higher fraction of *Ccl2* gene expression than F4/80-positive cells in both SD- and HFD-fed mice (Figure 4C). Similar result was obtained in *ob*/*ob* mice (Figures S3C and S3D).

To determine the inducers of adhesion molecules and chemokines, we examined the effects of tumor necrosis factor alpha (TNF-α), lipopolysaccharide (LPS), and palmitic acid on gene expression in cultured LSECs from WT mice. The genes of *Selp* and *Il6* were upregulated by treatment with LPS or palmitic acid, and those of *Icam1*, *Vcam1*, *Selp*, and *Ccl2* were induced by all factors (Figure 4D).

Obesity Enhances Myeloid Cell Adhesion and Transmigration across LSECs via VLA-4-Dependent Manner

We investigated the adherent function of LSECs in HFD-fed mice using flow-conditioned adhesion assays of mouse monocytes

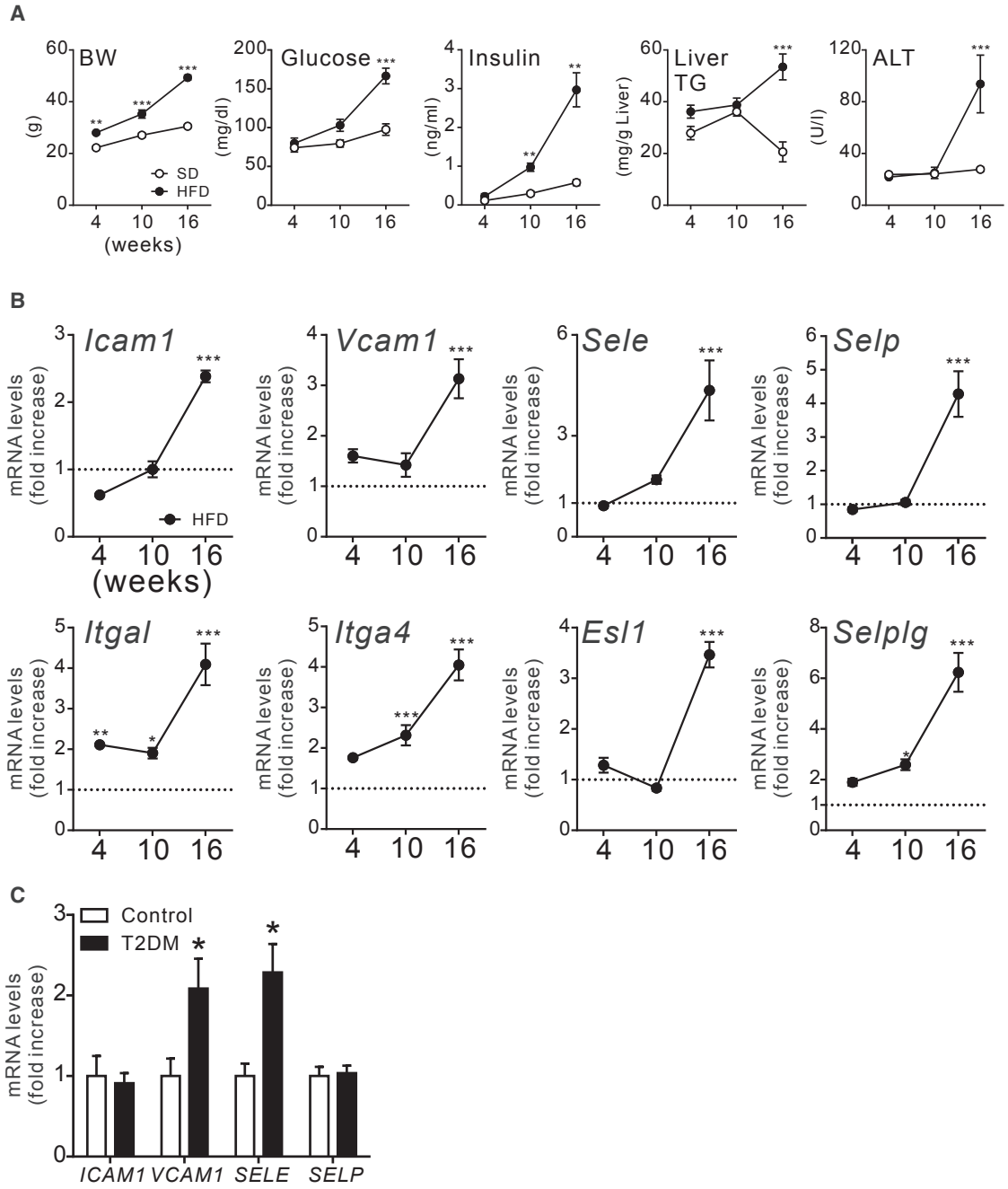

Figure 1. Changes in the Expression of Genes Related to Cell Adhesion Molecules in the Liver during the Development of Obesity

(A) Changes in body weight (BW) and levels of blood glucose, serum insulin, liver triglyceride (TG), and serum ALT in WT mice fed a SD and a high-fat diet (HFD) for 4, 10, and 16 weeks (n = 4).

(B) Changes in the levels of mRNA related to cell adhesion molecules and their ligands in the liver of mice fed an HFD for 4, 10, and 16 weeks, compared with those of control SD-fed mice (dotted lines).

(C) Relative mRNA levels of cell adhesion molecules in the liver of type 2 diabetes mellitus (T2DM, n = 10) and healthy individuals (control, n = 7) obtained from public microarray data.

All values represent mean ± SEM. *p < 0.05, **p < 0.01, ***p < 0.001 versus SD or control. See also Figure S1.

(WEHI 274.1 cells). Under physiologic flow rates in the hepatic sinusoids (Shetty et al., 2014), the number of rolling and adhesion cells to LSECs was markedly increased in HFD-fed mice compared with SD-fed mice (Figure 4E). When WEHI 274.1 cells were pretreated with blocking antibodies against integrins (LFA-1, VLA-4, or PSGL-1) (Balasa et al., 2015; Ji et al., 2011;

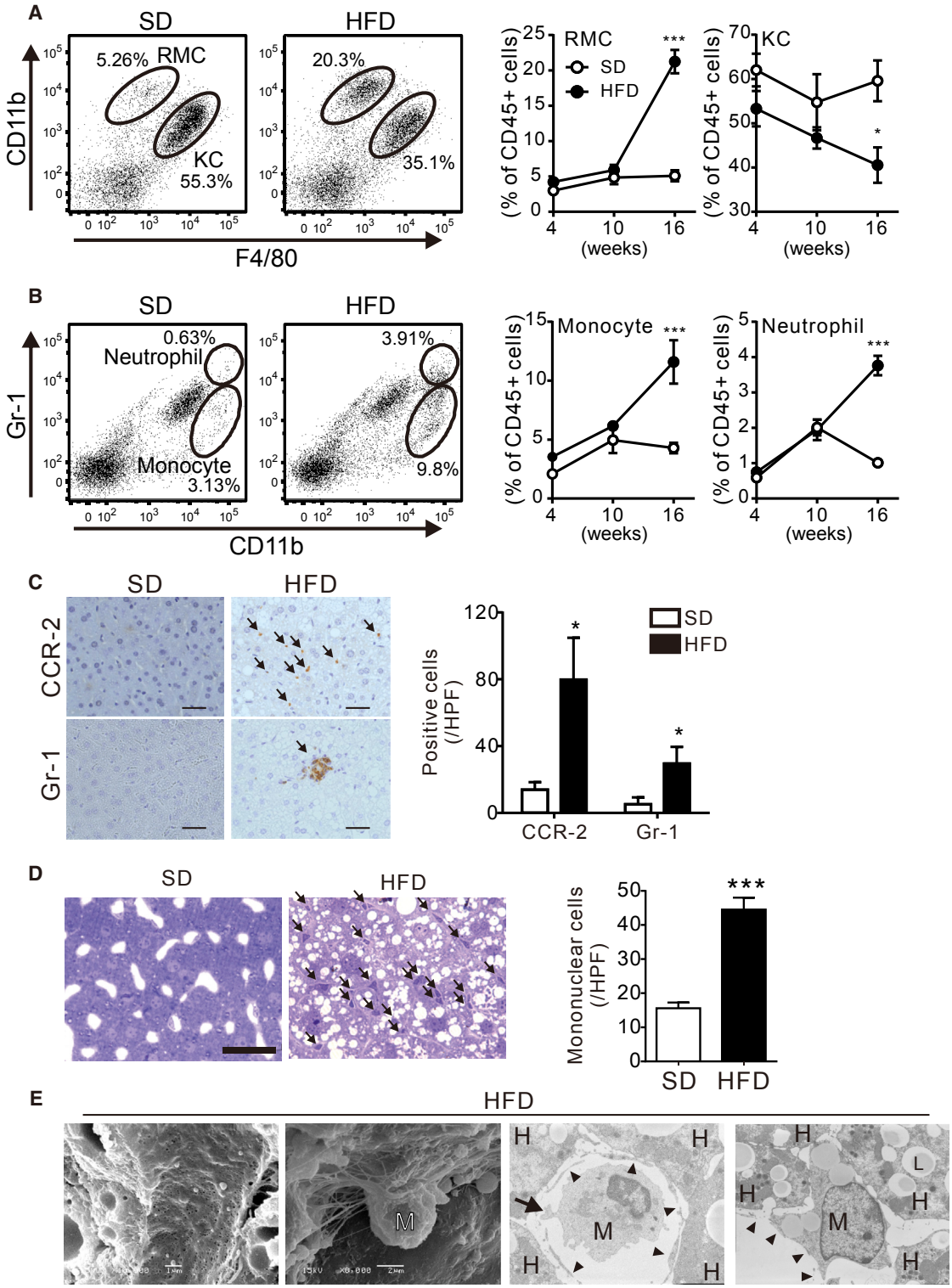

Figure 2. Myeloid Cell Accumulation in the Liver during the Development of Obesity

(A and B) Representative plots of flow cytometry for (A) recruited myeloid cells (RMCs) and Kupffer cells (KCs) and (B) neutrophils and monocytes in the liver from WT mice fed an SD and an HFD for 16 weeks. Quantification of flow cytometry in the liver from WT mice fed an SD and an HFD for 4, 10, and 16 weeks is shown (n = 4). Data are expressed as the percentage of $CD45^+$ cells in the liver non-parenchymal cells.

(legend continued on next page)

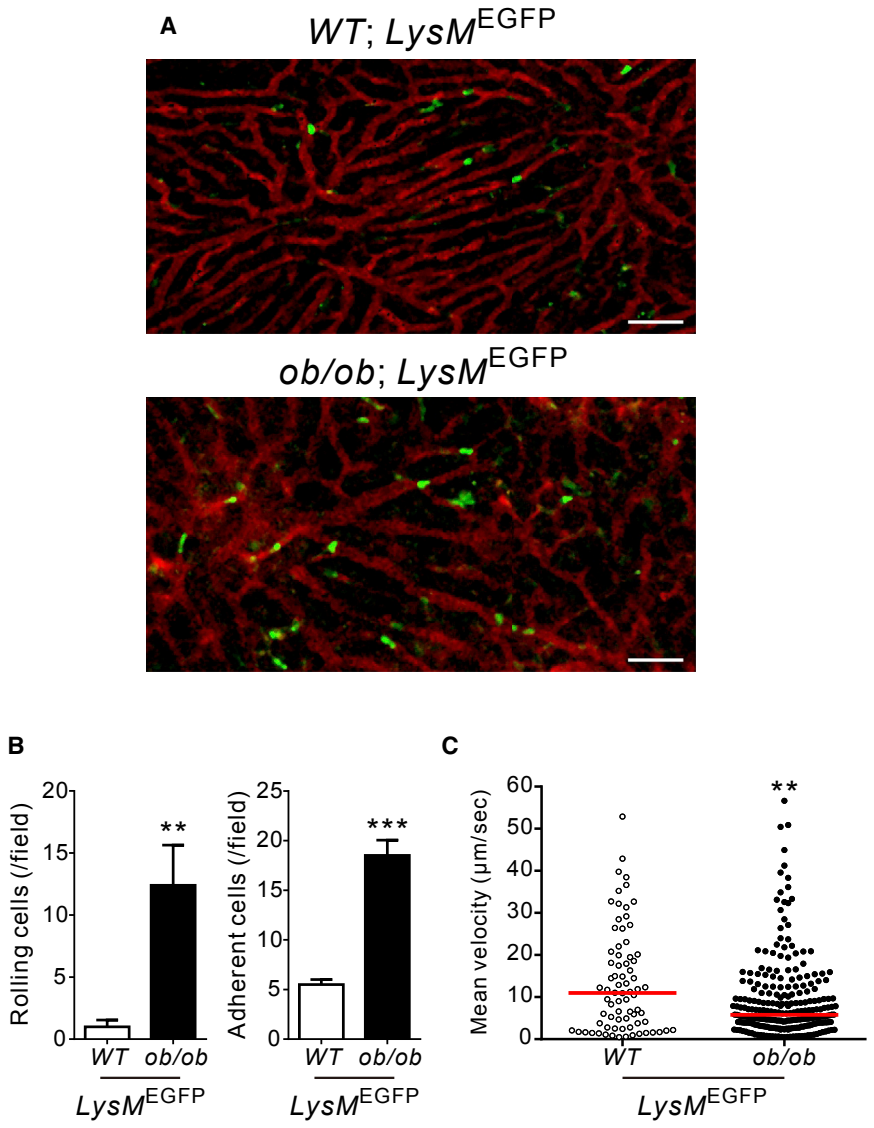

Figure 3. Intravital Imaging of Myeloid Cells in the Liver of Obese Mice

(A) Representative intravital multiphoton images of the liver in *LysM*^{EGFP} mice with WT or *ob/ob* background show EGFP-positive cells (green) and sinusoidal lumen (red). Scale bar, 50 μm.

(B) Quantification of EGFP-positive cells that rolled along and adhered to the sinusoidal wall of the liver in *LysM*^{EGFP} mice with WT (n = 40) or *ob/ob* background (n = 122). Values represent mean ± SEM.

(C) Quantification of mean velocities of EGFP-positive cells in 8-week-old of *LysM*^{EGFP} mice with WT (n = 76) or *ob/ob* (n = 253) background. The values (data points) and medians (bars) for individual cells compiled from three independent experiments are shown.

**p < 0.01, ***p < 0.001 versus *LysM*^{EGFP} mice with WT background. See also Movies S1 and S2.

Wang et al., 2012), monocyte adhesion to LSECs of HFD-fed mice was inhibited by anti-VLA-4 blocking antibody (Figure 4F). On transendothelial migration assays under static condition, VLA-4 blockade of WEHI 274.1 cells reduced cell transmigration across LSECs of HFD-fed mice (Figure 4G). We obtained similar data using LSECs of *ob/ob* mice (Figures S3E and S3F). Expression profiles of integrin genes in the sorted RMCs and Kupffer cells revealed that the gene of VLA-4 was dominantly expressed in RMCs compared with Kupffer cells (Figure 4H). Moreover, flow cytometry confirmed that the protein of VLA-4 is abundantly expressed in RMCs compared with Kupffer cells (Figure S3G).

Intravital imaging for *LysM*^{EGFP} mice with the *ob/ob* background showed that VLA-4 blockade inhibited transition of myeloid cells from the rolling to the adhesion state (Figures 5A and 5B). Consequently, VLA-4 blockade increased the mean velocity of hepatic myeloid cells in *LysM*^{EGFP} mice with *ob/ob* background (Figure 5C).

VLA-4 Blockade Attenuates Glucose Intolerance in Obesity Associated with Reduced RMC Accumulation

To examine the in vivo effects of VLA-4 on RMC accumulation and the metabolic changes, we administered intraperitoneal anti-VLA-4 blocking antibody or control immunoglobulin G (IgG) to SD- and HFD-fed mice for 6 weeks. For testing the specificity of anti-VLA-4 blocking antibody (clone: PS/2), liver non-parenchymal cells were pretreated with PS/2 antibody or isotype control IgG. Pretreatment of RMCs with PS/2 antibody blocked subsequent staining with anti-VLA-4 antibody (clone: R1-2), but not with anti-LFA-1 antibody (Figure S4A). In the SD-fed mice, VLA-4 blockade did not affect body weight, glucose tolerance, insulin sensitivity, and hepatic gene expression related to inflammation (Figures S4B–S4D). In

(C) Representative images and quantification of immunohistochemistry for CCR-2-positive and Gr-1-positive cells in the liver from mice that were fed an SD and an HFD for 16 weeks (400×; scale bar, 50 μm; n = 4). Arrows indicate immunopositive cells.

(D) Representative images and quantification of toluidine blue staining for mononuclear cells (arrows) in the liver from mice that were fed an SD and an HFD for 16 weeks (scale bar, 60 μm; n = 5–6).

(E) Representative images of scanning and transmission electron microscopy of liver sections from HFD-fed mice. From left to right, the sinusoidal wall, an activated monocyte adhered to the sinusoidal wall, a transmigrating monocyte, and a transmigrated macrophage among hepatocytes are shown. A protruding monocyte (arrow) and a layer of LSECs (arrowheads) are also shown.

All values represent mean ± SEM. *p < 0.05, ***p < 0.001 versus SD. H, hepatocyte; L, lipid droplet; M, monocyte or macrophage. See also Figure S2.

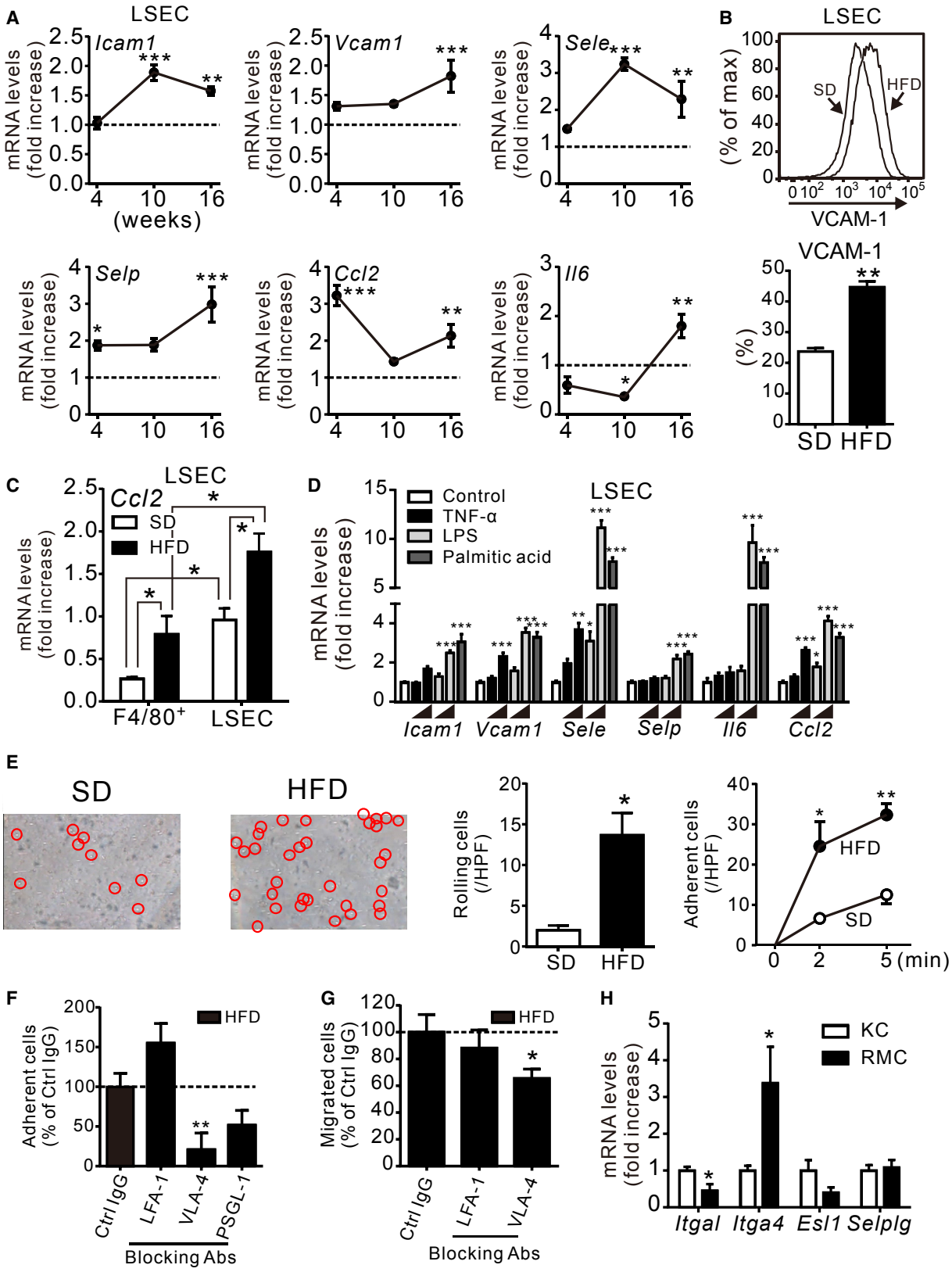

(legend on next page)

contrast, VLA-4 blockade significantly improved glucose intolerance and insulin sensitivity without affecting body weight (Figures 6A–6C). VLA-4 blockade also attenuated HFD-induced fasting hyperglycemia and hyperinsulinemia (Figures 6D and 6E). In the liver of HFD-fed mice, VLA-4 blockade attenuated the expression of inflammatory genes, including the gene of the RMC marker *Ccr2* (Figure 6F). Histologic analysis revealed that VLA-4 blockade reduced hepatic accumulation of CCR-2- and Gr-1-positive cells in HFD-fed mice (Figure 6G). There was a positive correlation between the number of CCR-2-positive cells and gene expression levels of *Tnf* in the liver (data not shown). Flow cytometry also demonstrated decreased accumulation of RMCs, monocytes, and neutrophils by VLA-4 blockade (Figures 6H and S4E). VLA-4 blockade did not affect serum lipid profile, liver TG content, or the expression of inflammatory genes in white adipose tissues of SD- and HFD-fed mice (data not shown).

Cell-Cell Contact between Intrahepatic Leukocytes and Hepatocytes Promotes Gluconeogenesis via a Notch-Dependent Pathway

We finally focused on the molecular mechanisms by which RMCs affect glucose metabolism in parenchymal hepatocytes. Pathway analysis of microarray data revealed that Notch signaling-related genes were upregulated in hepatocytes obtained from HFD-fed mice that were treated with control IgG, compared with both SD-fed and HFD-fed mice treated with anti-VLA-4 blocking antibody (Figure S5A). The Notch pathway, which involves ligands (Delta-like ligand [Dll] 1, Dll3, Dll4, Jagged1, and Jagged2) and receptors (Notch1–4), plays a critical role in the development of a variety of diseases (Bray, 2016). Cell-cell contract via Notch receptor-ligand interactions triggers the downstream responses, including the Notch transcriptional targets, such as the Hes-related (*Hes1*) and hairy enhancer of split (*Hey1*), and their family of genes. Compared with SD-fed mice, HFD-fed mice were found to have upregulated expression of Notch1 and production of the Notch receptor end product (Notch intracellular domain [NICD]) in hepatocytes, in which obesity contributes through p53 activation (Figures S5B and S5C) (Lefort et al., 2007). VLA-4 blockade decreased HFD-induced protein expression of NICD in isolated hepatocytes, as well as a gene of *Notch1* (Figures 7A and 7B). In hepatocytes, genetic or pharmacologic blockade of hepatic Notch signaling resulted in parallel inhibition of hepatic glucose production and glucose intolerance and was associated with downregulation of a gluconeogenic gene of glucose-6-phosphatase (*G6pc*) (Pajvani et al., 2011). Consistently, VLA-4 blockade significantly downregulated the Notch target genes (*Hes1* and *Hey1*) and *G6pc* in the liver or in isolated hepatocytes of HFD-fed mice (Figures 7B and 7C).

We hypothesized that RMCs trigger Notch signaling in hepatocytes via direct cell-cell contact. To evaluate the functional role of direct cell-cell contact between RMCs and hepatocytes in obesity-associated hepatic glucose intolerance, we carried out co-culture studies with direct cell-cell contact (direct co-culture) and transwell systems (transwell co-culture) (Figure S5D). Compared with transwell co-culture, direct co-culture of hepatic leukocytes (CD45-positive cells) with primary hepatocytes resulted to stronger induction of *Hey1*, *Hes1*, and *G6pc* expression (Figure 7D). Glucose concentration in conditioned media was higher in direct co-culture than in transwell co-culture (Figure 7E). Furthermore, insulin-induced suppression of cyclic AMP (cAMP)/dexamethasone (DEX)-induced *G6pc* upregulation was blunted in direct co-culture compared with transwell co-culture (Figure 7F). Luciferase reporter assays in Hepa 1–6 cells transfected with luciferase plasmids, which contained response elements of Notch nuclear effector CSL, revealed that direct co-culture of macrophages (RAW 264.7) increased CSL-luciferase activity in Hepa 1–6 cells; the extent of induction was dependent on the number of co-cultured macrophages (Figures 7G and 7H). Direct co-culture-induced CSL-luciferase activity was partially suppressed by pretreatment with two γ-secretase inhibitors (GSIs): Compound E and N-[N-(3,5-Difluorophenacetyl)-L-alanyl]-S-phenylglycine t-butyl ester (DAPT). However, JLK6, which is another GSI that inhibits only amyloid precursor protein cleavage without affecting Notch receptor cleavage (Petit et al., 2001), did not inhibit direct co-culture-induced CSL-luciferase activity (Figures 7H and S5E). Direct co-culture-induced expression of *Hey1*, *Hes1*, and *G6pc* was attenuated by pretreatment with Compound E (Figure 7I).

DISCUSSION

The liver is composed of parenchymal hepatocytes and stromal cells; hepatocytes represent 60%–70% of all liver cells, whereas

Figure 4. VLA-4-Mediated Adhesion and Transmigration of Myeloid Cells to LSECs

(A) Changes in the levels of mRNA of cell adhesion molecules, MCP-1 (*Ccl2*), and interleukin-6 (IL-6; *Il6*) in cultured LSECs from WT mice that were fed an SD and an HFD for 4, 10, and 16 weeks (n = 4).

(B) A representative plot and quantification of flow cytometry for VCAM-1 protein expression in LSECs from WT mice fed an SD and an HFD for 16 weeks (n = 3).

(C) Relative *Ccl2* mRNA levels in F4/80-positive cells and LSECs from the liver of mice that were fed an SD and an HFD (n = 4).

(D) mRNA levels of cytokines and adhesion molecules in cultured LSECs from WT mice after stimulation with TNF-α (1 or 10 ng/mL), LPS (1 or 10 ng/mL), or palmitic acid (250 μM) for 16 hr (n = 4).

(E) Representative images and quantification of parallel plate flow adhesion assays for rolling and adherent WEHI 274.1 cells (open red circles) on cultured LSECs from WT mice that were fed an SD and an HFD for 16 weeks. Quantification of rolling and adherence of WEHI 274.1 cells on LSECs at 5 min and at 2 and 5 min of perfusion, respectively (n = 3).

(F) The cumulative number of WEHI 274.1 cells adherent to LSECs of HFD-fed mice during 5 min of perfusion after pretreatment with blocking antibody against LFA-1, VLA-4, PSGL-1, or control (Ctrl) IgG (n = 3).

(G) Quantification of WEHI 274.1 cells that transmigrated across LSECs of HFD-fed mice after pretreatment with blocking antibody against LFA-1, VLA-4, PSGL-1, or control (Ctrl) IgG (n = 3).

(H) mRNA levels in isolated Kupffer cells (KCs) and RMCs from the liver of SD-fed WT mice (n = 3).

Values represent mean ± SEM. *p < 0.05, **p < 0.01, ***p < 0.001 versus SD or control. See also Figure S3 and Movie S3.

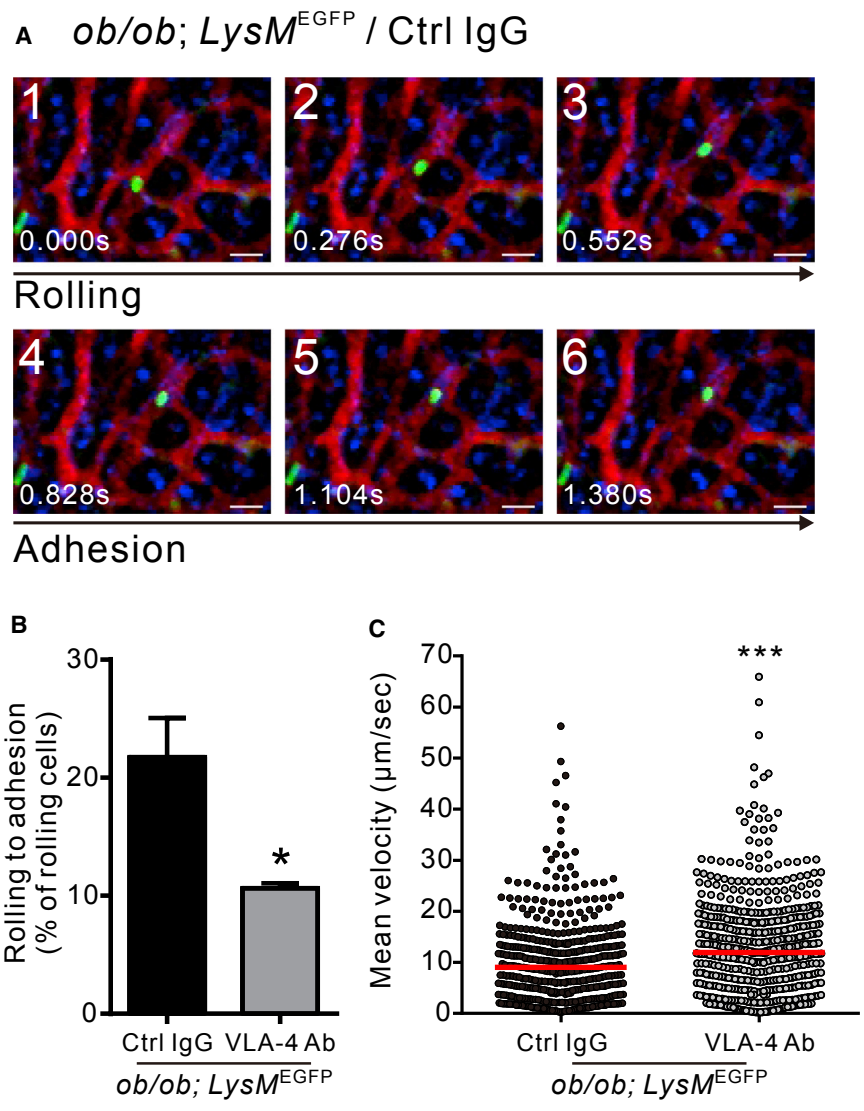

Figure 5. Intravital Imaging of VLA-4-Mediated Adhesion of Myeloid Cells to Liver Sinusoidal Wall in Obese Mice

(A) Representative sequential images of intravital multiphoton images of the liver in *LysM*^{EGFP} mice with *ob/ob* background. A rolling (Nos. 1–3) and adherent (Nos. 4–6) EGFP-positive cell (green) to the sinusoidal lumen (red) is shown. Scale bar, 20 μm.

(B) Quantification of EGFP-positive cells transitioning from the rolling to the adherent state in the liver of *LysM*^{EGFP} mice with *ob/ob* background, which was pretreated with control (Ctrl) IgG or anti-VLA-4 blocking antibody (n = 3). Values represent mean ± SEM. **p < 0.01 versus Ctrl IgG.

(C) Quantification of mean velocities of EGFP-positive cells in *LysM*^{EGFP} mice with *ob/ob* background, which were pretreated with Ctrl IgG (n = 476) or anti-VLA-4 blocking antibody (n = 553). The values (data points) and medians (bars) for individual cells compiled from three independent experiments are shown.

***p < 0.001 versus *LysM*^{EGFP} mice with *ob/ob* background pretreated with Ctrl IgG. See also Movie S4.

stromal cells include LSECs, RMCs, Kupffer cells, and hepatic stellate cells. It has been reported that cell-cell interactions between parenchymal and stromal cells play crucial roles in a variety of physiologic and pathologic responses in the liver, such as regeneration (Forbes and Rosenthal, 2014; Rafii et al., 2016), viral hepatitis (Guidotti and Chisari, 2006), fibrosis (Rockey et al., 2015), and hepatocellular carcinoma (Drucker et al., 2006). In the present study, we demonstrated cell-cell adhesion and contact between parenchymal and stromal cells during the development of obesity-associated hepatic inflammation and glucose intolerance. In addition to parenchymal hepatocyte dysfunction by cell autonomous mechanisms, insight into the cellular and molecular mechanisms underlying hepatic glucose metabolism in stromal cells is provided by our study, suggesting intrahepatic cell-cell adhesion and contact as potential therapeutic targets for obesity-associated glucose intolerance.

In this study, intravital imaging enabled observation of the dynamics of myeloid cells in the liver of obese mice: obesity markedly increased the number of rolling and adherent myeloid cells on the sinusoidal wall, and VLA-4 blockade significantly reduced the transition from rolling to adherence. All these observations were confirmed by ex vivo experiments under flow conditions. Previous papers have shown that cell-cell adhesion between leukocytes and LSECs was upregulated in various liver diseases and stimuli, including nonalcoholic fatty liver disease (Miyao et al., 2015), viral hepatitis (Volpes et al., 1990), endotoxemia (McDonald et al., 2008), and mechanical injury (McDonald et al., 2010). Although adhesive determinants between leukocytes and LSECs varied among pathologic situations, increased cell adhesion has consistently been reported to promote infiltration of myeloid cells. Moreover, VLA-4 and its counter-receptor VCAM-1 in the liver have been shown to be responsible for leukocyte infiltration during ischemia-reperfusion injury (Jaeschke, 2006). Consistent with our study, a previous paper has shown that mice globally bearing a mutation of VLA-4 (Y991A), which blocks VLA-4-mediated leukocyte migration (Liu et al., 1999), protected HFD-fed mice from hyperglycemia and insulin resistance (Féral et al., 2008). Furthermore, this protection was observed in WT mice after bone marrow transplantation from the mutant mice. Therefore, although that paper did not show detailed liver phenotypes, the improved glucose metabolism may have been partly mediated by reduced intrahepatic cell-cell adhesion via VLA-4.

LSECs are directly exposed to cytokines and fatty acids that are released by portally drained intra-abdominal adipose tissues. In the present study, TNF-α, LPS, and palmitate, which

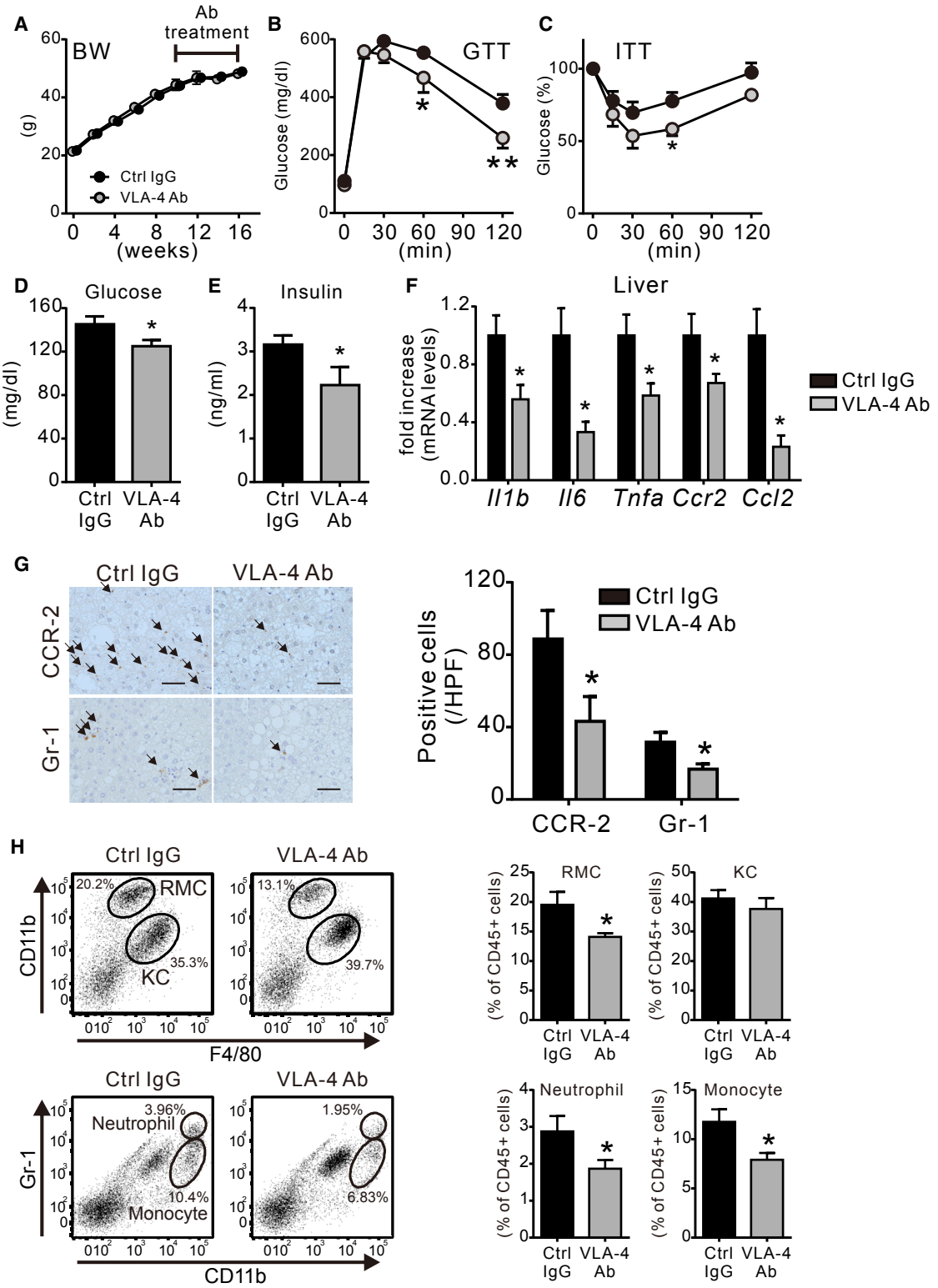

Figure 6. Glucose Metabolism and Myeloid Cell Accumulation in the Liver after Treatment with Anti-VLA-4 Blocking Antibody

(A) Changes in body weight in 6-week-old WT mice during HFD feeding for 16 weeks. After 10 weeks of HFD, anti-VLA-4 blocking antibody (VLA-4 Ab) or isotype control (Ctrl) IgG was intraperitoneally injected (n = 6–8).

(legend continued on next page)

were reported to have increased intraportal concentration in obesity (Item and Konrad, 2012), induced genes of adhesion molecules and chemokines, such as *Vcam1* and *Ccl2*, in cultured LSECs from WT mice. Therefore, these intraportal soluble factors could be inducers of these genes in the LSECs of obese mice. Because a previous paper showed that hepatocyte-derived factors could promote leukocyte adhesion and transmigration through upregulation of adhesion molecules in LSECs (Edwards et al., 2005), some hepatocyte-derived factors affected by obesity could also induce these genes in LSECs. In addition, we have shown that a sodium-glucose co-transporter 2 (SGLT2) inhibitor, ipragliflozin, attenuated HFD-induced upregulation of these genes in the liver. Our previous paper has shown that 4-week treatment of an SGLT2 inhibitor prevents hyperglycemia, hyperinsulinemia, and hepatic steatosis in HFD-fed mice (Komiya et al., 2016). Therefore, it also suggests that these factors inhibited by the SGLT2 inhibitor can contribute to the induction of these genes. The detailed mechanism of how these factors regulate the genes of cytokines and adhesion molecules in LSECs awaits further studies.

The present study demonstrated that VLA-4 blockade in obese mice improved glucose intolerance, with reduced RMC accumulation and inflammatory gene expression in the liver. Similar to adipose tissue, hepatocytes are predisposed to inflammation by obesity; this fact was reflected by increased production of tissue inflammatory cytokines (Glass and Olefsky, 2012; Osborn and Olefsky, 2012). At the cellular level, there is considerable evidence that RMCs have a significant role in obesity-associated hepatic inflammation and glucose intolerance. For instance, deletion of IκB kinase β in myeloid cells was shown to inhibit macrophage-mediated inflammation and to improve hepatic insulin sensitivity with reduction of hepatic inflammation (Arkan et al., 2005; Cai et al., 2005). Overexpression of MCP-1 in the liver increased RMC accumulation to promote systemic insulin resistance and hepatic inflammation (Obstfeld et al., 2010). Obesity also promotes neutrophil accumulation in the liver, and neutrophil-derived elastase induces glucose intolerance through degradation of hepatic insulin receptor substrate 1 (Talukdar et al., 2012). Therefore, attenuation of RMC-derived inflammatory cytokines, and possibly other bioactive molecules, by reduced RMC accumulation may be one of the major mechanisms by which VLA-4 blockade improved glucose intolerance in obese mice.

As another mechanism by which RMCs promote glucose intolerance, cell-cell contact between intrahepatic leukocytes and hepatocytes was shown in this study to promote gluconeogenesis through a Notch-dependent pathway. In HFD-fed mice, VLA-4 blockade reduced hepatocyte Notch activity, as assessed by NICD expression, and decreased RMC accumulation. Activation of Notch signaling is unidirectional; a signal-sending cell, which represents the Notch ligand, comes into contact with the signal-receiving cell, which expresses the Notch receptor (Bray, 2016). Although inhibition of hepatic Notch signaling has been demonstrated to protect mice from obesity-induced glucose intolerance by suppressing *G6pc* expression and hepatic glucose output (Pajvani et al., 2011), the signal-sending cells have not been identified in that state. Given our histologic observation that RMCs were localized not only in the sinusoidal lumen adherent to the LSECs but also among hepatocytes after transendothelial migration, the RMCs that infiltrate hepatocytes could be the signal-sending cells that trigger Notch signaling in the neighboring hepatocytes. The significance and detailed mechanisms of RMC-mediated activation of hepatic Notch signaling require further in vivo studies.

Resident Kupffer cells were reported to play a significant role in obesity-associated hepatic inflammation and glucose intolerance; an HFD in mice induced inflammatory activation of Kupffer cells (Lanthier et al., 2010), and chemical deletion of Kupffer cells was demonstrated to improve obesity-induced hyperglycemia associated with reduced hepatic inflammation (Huang et al., 2010). However, in the present study, VLA-4 blockade did not change the absolute number and level of expression of inflammatory genes of Kupffer cells. Based on this observation, Kupffer cells were less likely to contribute to the improvement of glucose intolerance than the reduced RMC accumulation by VLA-4 blockade. In addition, we have shown that, compared with F4/80-positive cells in liver, LSECs accounted for a higher fraction of *Ccl2* gene expression in both SD- and HFD-fed mice. Therefore, LSECs could be significant sources of MCP-1 expression in the liver for recruitment of myeloid cells. Vascular endothelial cell-derived MCP-1 has been demonstrated to play a crucial role in initiating atherosclerosis by recruiting macrophages and monocytes to the vessel wall (Gu et al., 1998). MCP-1 has been also shown to enhance VLA-4-dependent adhesion and chemotaxis in a human monocytic cell line (Ashida et al., 2001). Altogether, LSEC-derived MCP-1 might have a significant role in RMC recruitment and accumulation to induce hepatic inflammation.

The reasons RMCs infiltrate into liver remain unclear. In liver, obesity increases hepatocyte apoptosis in mice (Abdelmegeed et al., 2011; Hillian et al., 2013; Meakin et al., 2014; Park et al., 2014). In the present study, RMCs, especially infiltrated neutrophils ($Gr\text{-}1^{+}$), appeared to show focal aggregation in the liver of HFD-fed mice. From these observations, we speculate that a possible role of the RMCs is to remove dying or dead hepatocytes in obese subjects. We also consider that hepatic insulin

(B and C) Intraperitoneal (B) glucose tolerance test (GTT) and (C) insulin tolerance test (ITT) on HFD-fed mice after treatment with VLA-4 Ab for 5 weeks or with Ctrl IgG for 4 weeks.
(D and E) Fasting (D) blood glucose and (E) serum insulin levels in HFD-fed mice after treatment with VLA-4 Ab and Ctrl IgG for 6 weeks.
(F) mRNA levels in the liver from HFD-fed mice after treatment with VLA-4 Ab and Ctrl IgG for 6 weeks.
(G) Representative images and quantification of immunohistochemistry for CCR-2 and Gr-1 in the liver of HFD-fed mice after treatment with VLA-4 Ab and Ctrl IgG for 6 weeks (400×; Scale bar, 50 μm). Arrows indicate immunopositive cells.
(H) Representative plots and quantification of flow cytometry for RMCs, Kupffer cells (KCs), neutrophils, and monocytes in the liver of HFD-fed mice treated with VLA-4 Ab or Ctrl IgG for 6 weeks. Data are expressed as a percentage of $CD45^{+}$ cells in the non-parenchymal cells of the liver.
All values represent mean ± SEM. *$p < 0.05$, **$p < 0.01$ versus Ctrl IgG or indicated groups. See also Figure S4.

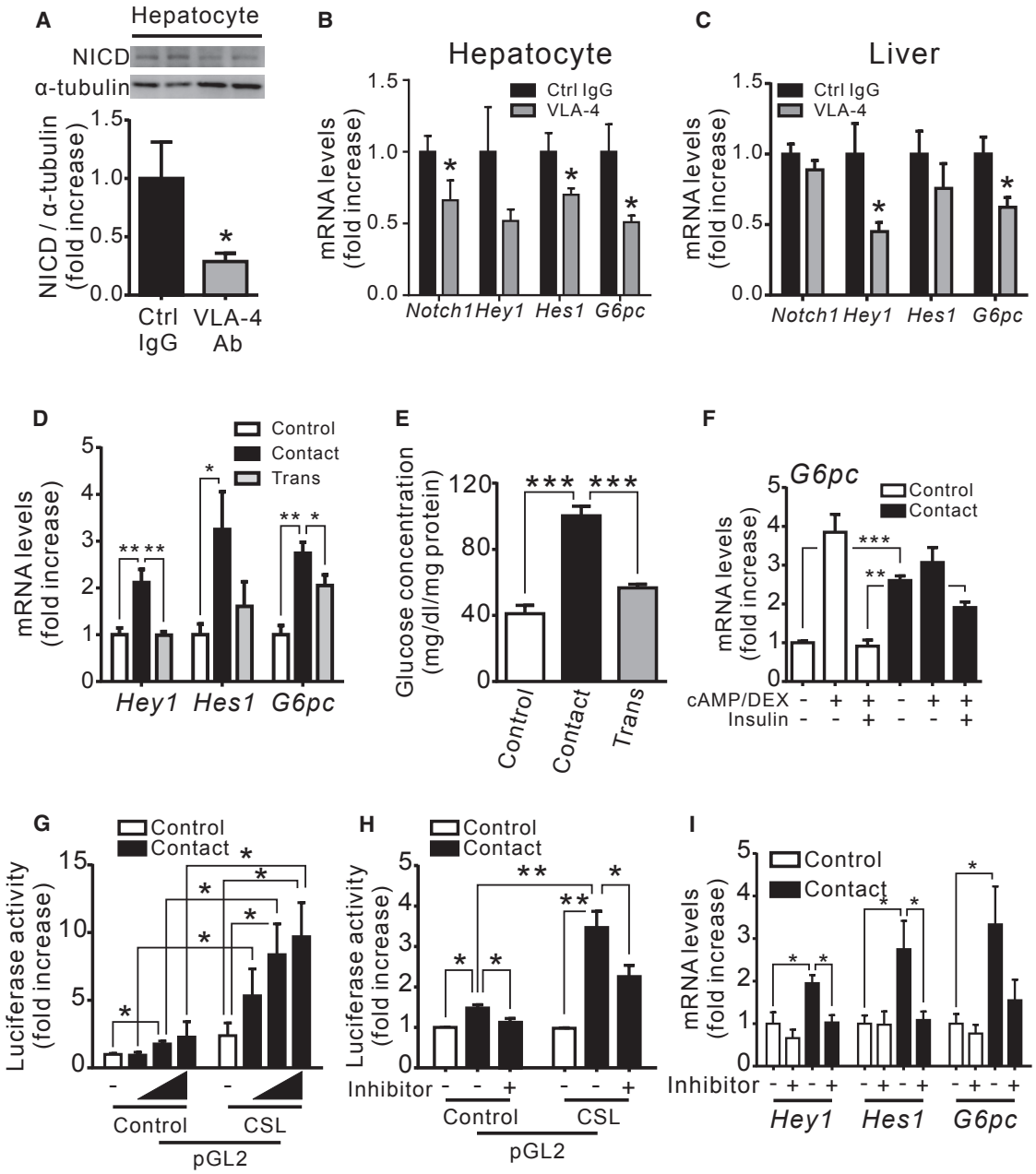

Figure 7. Stimulation of Glucose Production by Cell-Cell Contact via a Notch-Dependent Pathway

(A) Representative immunoblot images and quantification of protein expression of Notch intracellular domain (NICD) in hepatocytes isolated from HFD-fed mice treated with anti-VLA-4 blocking antibody (VLA-4 Ab) and control (Ctrl) IgG for 6 weeks (n = 6–8).

(B and C) α-tubulin was used as an internal control. mRNA levels in the (B) isolated hepatocytes and (C) liver of HFD-fed mice after treatment with VLA-4 Ab and Ctrl IgG for 6 weeks (n = 6–8).

(D and E) Comparison of mRNA levels of Notch target genes and *G6pc* (D) and glucose production in direct or transwell co-culture systems (E) between primary hepatocytes and intrahepatic leukocytes (n = 4).

(F) mRNA levels of *G6pc* in primary hepatocytes co-cultured with intrahepatic leukocytes, followed by incubation with cAMP/DEX, with or without 10 nM insulin, for 4 hours (n = 4).

(G and H) CSL-luciferase activity in Hepa 1–6 cells co-cultured with (G) different numbers of RAW 264.7 cells (1/100, 1/10, and 1/1 cells to Hepa 1–6 cells) and (H) RAW 264.7 cells pretreated with or without Notch inhibitor Compound E (inhibitor, 10 μM) (n = 4).

(I) mRNA levels in a mixture of primary hepatocytes and RAW 264.7 cells that were pretreated with or without Notch inhibitor Compound E (inhibitor, 1 μM) (n = 4).

All values represent mean ± SEM. *p < 0.05, **p < 0.01, ***p < 0.001 versus control or indicated groups. See also Figure S5.

resistance and glucose intolerance are a result of RMCs accumulation, via RMC-derived bioactive molecules and cell-cell contact to hepatocytes. Other pathophysiologic significances and roles of RMCs await further study.

Notch signaling creates a positive feedback loop, named lateral induction, wherein Notch activation in one cell induces the expression of the Notch-activating ligand in the same cell (Bray, 2016). As a result, a cluster of cells could cooperatively activate Notch and express the signaling ligand uniformly. Along with our observation that genes of Notch receptors and ligands were upregulated in hepatocytes of HFD-fed mice, it is conceivable that a relatively small number of RMCs could activate Notch signaling in a large number of hepatocytes. The detailed process of intercellular propagation of Notch signaling in the liver requires further investigation.

In conclusion, our study revealed mechanisms of hepatic glucose metabolism regulated by physical cell-cell interaction of RMCs with LSECs or hepatocytes. Based on these insights into the pathogenesis of obesity-associated hepatic inflammation and abnormal glucose metabolism, intrahepatic physical cell-cell interaction might be a potential therapeutic target against obesity-induced glucose intolerance.

EXPERIMENTAL PROCEDURES

Additional details of the experimental procedures are included in the Supplemental Information section.

Animal Experiments

All animal experiments were approved by the Tokyo Medical and Dental University Committee on Animal Research (No. 0170111A). Male WT C57BL/6J mice were obtained from CLEA Japan. C57BL/6J-*ob*/*ob* (*ob*/*ob*) mice were purchased from Japan SLC. All animals were fed a SD or a HFD (60% of calories from fat; D12492, Research Diets). Mice were maintained on a 12-hr light and 12-hr dark cycle with free access to food and water. For treatment with anti-VLA-4 blocking antibody, rat anti-mouse VLA-4 monoclonal antibody (120 μg per injection; clone: PS/2, Bio X Cell) or control rat IgG2bκ (120 μg per injection) was intraperitoneally injected to WT mice twice a week for 6 weeks. Oral administration of ipragliflozin to *ob*/*ob* or HFD-fed WT mice was performed, as previously reported (Komiya et al., 2016).

Metabolic Analysis

Blood glucose and plasma insulin concentrations were measured with a glucometer (Glutest Pro R, Sanwa Kagaku) and ELISA (Morinaga), respectively. Liver triglyceride (TG) content was determined, as previously described (Komiya et al., 2016). TG, total cholesterol (TC), free fatty acid (FFA), and ALT were measured at Ikagaku. For glucose tolerance tests, mice were fasted for 16 hr with free access to water, followed by intraperitoneal glucose injection (2 g/kg). For insulin tolerance tests, 2-hr fasted mice were intraperitoneally injected with human insulin (1.0 U/kg). We measured blood glucose concentrations at 0, 15, 30, 60, and 120 min after injection.

Multiphoton Intravital Liver Tissue Imaging

Intravital liver tissue imaging was originally established. Briefly, 15- to 20-week-old, *LysM*^{EGFP} (Faust et al., 2000) mice were anesthetized with isoflurane (Escain; 2.0% vaporized in 100% oxygen). After making an incision of the skin and peritoneum just under the xiphoid process, the median lobe of the liver was exposed. The liver was gently put on a cover glass attached to a custom-made holder and immobilized by gluing three spots to prevent drifting of visual field. Then the internal surface was observed by inverted two-photon excitation microscopy. The imaging system was composed of a two-photon microscope (A1-MP, Nikon) driven by a laser (Chameleon Vision II Ti:Sapphire, Coherent) tuned to 880 nm and an inverted microscope equipped with a water multi-immersion objective lens (Plan Fluor, 0.75 numerical aperture [NA], Nikon). Nuclei and vessels were visualized by intravenous injection of Hoechst 33342 (Thermo Fisher Scientific) and Qtracker 655 (Thermo Fisher Scientific) immediately before imaging. Fluorescent signals were detected through band-pass emission filters at 492/SP nm (for Hoechst 33342), 525/50 nm (for EGFP), and 660/52 nm (for Qtracker 655). For examining the effect of anti-VLA-4 blocking antibody, rat anti-mouse VLA-4 monoclonal antibody (200 μg per injection) or control rat IgG2bκ (200 μg per injection) was intravenously administered 4 hr before imaging. Raw imaging data were processed with NIS-Elements (Nikon). Data were analyzed by NIH ImageJ software. EGFP-positive cells were tracked with TrackMate in Fiji (ImageJ) and were considered adherent to the sinusoidal wall when they remained stationary for at least eight frames (about 1 s). Mean velocity of the tracked cells was calculated using TrackMate.

Electron Microscopy

Mouse livers were perfused via the portal vein with normal saline, followed by 2.5% glutaraldehyde ([pH 7.4], in 0.1 M phosphate buffer) for 5 min. The protocol of transmission electron microscopy was previously described (Inoue et al., 2012; Scheibye-Knudsen et al., 2014). Liver tissues were post-fixed in 2% osmium tetroxide for 1 hr at 4°C, dehydrated, and embedded in epoxy resin (Epon 812). Semi-thin sections were stained with 1% toluidine blue to trim selected areas and to assess the number and localization of mononuclear cells. Ultra-thin (60–90 nm) sections were stained with uranyl acetate, followed by lead citrate, and were examined on an 80-kV JEM 1200EX electron microscope (JEOL). For scanning electron microscopy (JSM 5600LV, JEOL), perfused liver tissues were crushed under liquid nitrogen, osmicated, dehydrated, mounted, and coated with gold.

Parallel Plate Flow Chamber Adhesion Assay

The parallel plate flow chamber was used as described previously (Edwards et al., 2005). LSECs were placed onto 22-mm collagen-coated glass coverslips and incubated overnight at 37°C. Cells were positioned in a flow chamber mounted on a Nikon inverted microscope. WEHI 274.1 cells (1×10^7/mL) were incubated with monoclonal antibody for 15 min at 4°C, diluted 10-fold in the perfusion medium (PBS with Ca^{2+} and Mg^{2+} containing 0.2% BSA), and passed through the chamber with a syringe pump (PHD2000, Harvard Apparatus) for 5 min at a shear stress of 0.5 dyne/cm^2 (Clark et al., 2007). The monoclonal antibodies used were anti-LFA-1 (10 μg/mL, clone: M17/4, BioLegend), anti-VLA-4 (10 μg/mL, clone: PS/2, Bio X Cell), anti-PSGL-1 (10 μg/mL, clone: 4RA10, Bio X Cell), and control IgG (10 μg/mL). Ten randomly selected fields (200×) were recorded for 30 s. Rolling cells were identified as those with a rolling motion and a slower velocity than the flow stream (Shetty et al., 2014). Adherent cells were defined as those that firmly adhered to the endothelial layer for at least 5 s until the end of a 30-s time frame. The total number of rolling and adherent cells was counted in each field and was compared between control chambers and those treated with blocking antibodies.

Statistical Analysis

All data were analyzed using GraphPad Prism 6 and were presented as mean ± SEM. A p value < 0.05 was considered statistically significant. Unpaired t test or Mann-Whitney U test was used to compare two groups. One-way or two-way ANOVA, followed by a post-hoc test, was used for comparison of more than two groups.

ACCESSION NUMBERS

The accession numbers for the microarray data reported in this paper are GEO: GSE84019 and GSE85673.

SUPPLEMENTAL INFORMATION

Supplemental Information includes Supplemental Experimental Procedures, five figures, and four movies and can be found with this article online at http://dx.doi.org/10.1016/j.celrep.2017.02.039.

AUTHOR CONTRIBUTIONS

Y.M. and K.T. designed the experiments. Y.M., C.K., K.S., N.S., S.Y., M.D., M.O., K.I., Y.S., S.M., and J.K. conducted the experiments. Y.M. and K.T. analyzed data. M.O., J.K., and K.W. contributed to interpretation of data. Y.M., K.T., J.K., and Y.O. wrote the paper. K.T., K.W., M.Y., M.I., and Y.O. supervised the study.

ACKNOWLEDGMENTS

This work was supported in part by grants-in-aid for scientific research from the Ministry of Education, Culture, Sports, Science and Technology of Japan. Y.M. was the recipient of the Junior Scientist Development Grant of JDS by Novo Nordisk Pharma. K.T. was the recipient of Uehara Memorial Foundation research fellowship, Japan Diabetes Foundation fellowship, Banyu Foundation research grant, and a grant of the Japan Foundation for Applied Enzymology. Y.O. was funded by the Japan Agency for Medical Research and Development, Core Research for Evolutional Science and Technology (AMED-CREST), and Uehara Memorial Foundation.

Received: October 21, 2016
Revised: January 18, 2017
Accepted: February 13, 2017
Published: March 14, 2017

REFERENCES

Abdelmegeed, M.A., Yoo, S.H., Henderson, L.E., Gonzalez, F.J., Woodcroft, K.J., and Song, B.J. (2011). PPARalpha expression protects male mice from high fat-induced nonalcoholic fatty liver. J. Nutr. *141*, 603–610.

Arkan, M.C., Hevener, A.L., Greten, F.R., Maeda, S., Li, Z.W., Long, J.M., Wynshaw-Boris, A., Poli, G., Olefsky, J., and Karin, M. (2005). IKK-beta links inflammation to obesity-induced insulin resistance. Nat. Med. *11*, 191–198.

Ashida, N., Arai, H., Yamasaki, M., and Kita, T. (2001). Distinct signaling pathways for MCP-1-dependent integrin activation and chemotaxis. J. Biol. Chem. *276*, 16555–16560.

Balasa, B., Yun, R., Belmar, N.A., Fox, M., Chao, D.T., Robbins, M.D., Starling, G.C., and Rice, A.G. (2015). Elotuzumab enhances natural killer cell activation and myeloma cell killing through interleukin-2 and TNF-α pathways. Cancer Immunol. Immunother. *64*, 61–73.

Bray, S.J. (2016). Notch signalling in context. Nat. Rev. Mol. Cell Biol. *17*, 722–735.

Cai, D., Yuan, M., Frantz, D.F., Melendez, P.A., Hansen, L., Lee, J., and Shoelson, S.E. (2005). Local and systemic insulin resistance resulting from hepatic activation of IKK-beta and NF-kappaB. Nat. Med. *11*, 183–190.

Clark, S.R., Ma, A.C., Tavener, S.A., McDonald, B., Goodarzi, Z., Kelly, M.M., Patel, K.D., Chakrabarti, S., McAvoy, E., Sinclair, G.D., et al. (2007). Platelet TLR4 activates neutrophil extracellular traps to ensnare bacteria in septic blood. Nat Med. *13*, 463–469.

Drucker, C., Parzefall, W., Teufelhofer, O., Grusch, M., Ellinger, A., Schulte-Hermann, R., and Grasl-Kraupp, B. (2006). Non-parenchymal liver cells support the growth advantage in the first stages of hepatocarcinogenesis. Carcinogenesis *27*, 152–161.

Edwards, S., Lalor, P.F., Nash, G.B., Rainger, G.E., and Adams, D.H. (2005). Lymphocyte traffic through sinusoidal endothelial cells is regulated by hepatocytes. Hepatology *41*, 451–459.

Faust, N., Varas, F., Kelly, L.M., Heck, S., and Graf, T. (2000). Insertion of enhanced green fluorescent protein into the lysozyme gene creates mice with green fluorescent granulocytes and macrophages. Blood *96*, 719–726.

Féral, C.C., Neels, J.G., Kummer, C., Slepak, M., Olefsky, J.M., and Ginsberg, M.H. (2008). Blockade of alpha4 integrin signaling ameliorates the metabolic consequences of high-fat diet-induced obesity. Diabetes *57*, 1842–1851.

Forbes, S.J., and Rosenthal, N. (2014). Preparing the ground for tissue regeneration: from mechanism to therapy. Nat. Med. *20*, 857–869.

Glass, C.K., and Olefsky, J.M. (2012). Inflammation and lipid signaling in the etiology of insulin resistance. Cell Metab. *15*, 635–645.

Gu, L., Okada, Y., Clinton, S.K., Gerard, C., Sukhova, G.K., Libby, P., and Rollins, B.J. (1998). Absence of monocyte chemoattractant protein-1 reduces atherosclerosis in low density lipoprotein receptor-deficient mice. Mol. Cell *2*, 275–281.

Guidotti, L.G., and Chisari, F.V. (2006). Immunobiology and pathogenesis of viral hepatitis. Annu. Rev. Pathol. *1*, 23–61.

Hillian, A.D., McMullen, M.R., Sebastian, B.M., Roychowdhury, S., Kashyap, S.R., Schauer, P.R., Kirwan, J.P., Feldstein, A.E., and Nagy, L.E. (2013). Mice lacking C1q are protected from high fat diet-induced hepatic insulin resistance and impaired glucose homeostasis. J. Biol. Chem. *288*, 22565–22575.

Huang, W., Metlakunta, A., Dedousis, N., Zhang, P., Sipula, I., Dube, J.J., Scott, D.K., and O'Doherty, R.M. (2010). Depletion of liver Kupffer cells prevents the development of diet-induced hepatic steatosis and insulin resistance. Diabetes *59*, 347–357.

Inoue, K., Hara, Y., and Sato, T. (2012). Development of the oxytalan fiber system in the rat molar periodontal ligament evaluated by light- and electron-microscopic analyses. Ann. Ata. *194*, 482–488.

Item, F., and Konrad, D. (2012). Visceral fat and metabolic inflammation: the portal theory revisited. Obes. Rev. *13*, 30–39.

Jaeschke, H. (2006). Mechanisms of liver injury. II. Mechanisms of neutrophil-induced liver cell injury during hepatic ischemia-reperfusion and other acute inflammatory conditions. Am. J. Physiol. Gastrointest. Liver Physiol. *290*, G1083–G1088.

Ji, N., Rao, N., Guentzel, N.M., Arulanandam, B.P., and Forsthuber, T.G. (2011). Anaphylaxis and mortality induced by treatment of mice with anti-VLA-4 antibody and pertussis toxin. J. Immunol. *186*, 2750–2756.

Jia, L., Vianna, C.R., Fukuda, M., Berglund, E.D., Liu, C., Tao, C., Sun, K., Liu, T., Harper, M.J., Lee, C.E., et al. (2014). Hepatocyte Toll-like receptor 4 regulates obesity-induced inflammation and insulin resistance. Nat. Commun. *5*, 3878.

Komiya, C., Tsuchiya, K., Shiba, K., Miyachi, Y., Furuke, S., Shimazu, N., Yamaguchi, S., Kanno, K., and Ogawa, Y. (2016). Ipragliflozin improves hepatic steatosis in obese mice and liver dysfunction in type 2 diabetic patients irrespective of body weight reduction. PLoS ONE *11*, e0151511.

Lanthier, N., Molendi-Coste, O., Horsmans, Y., van Rooijen, N., Cani, P.D., and Leclercq, I.A. (2010). Kupffer cell activation is a causal factor for hepatic insulin resistance. Am. J. Physiol. Gastrointest. Liver Physiol. *298*, G107–G116.

Lefort, K., Mandinova, A., Ostano, P., Kolev, V., Calpini, V., Kolfschoten, I., Devgan, V., Lieb, J., Raffoul, W., Hohl, D., et al. (2007). Notch1 is a p53 target gene involved in human keratinocyte tumor suppression through negative regulation of ROCK1/2 and MRCKalpha kinases. Genes Dev. *21*, 562–577.

Liu, S., Thomas, S.M., Woodside, D.G., Rose, D.M., Kiosses, W.B., Pfaff, M., and Ginsberg, M.H. (1999). Binding of paxillin to alpha4 integrins modifies integrin-dependent biological responses. Nature *402*, 676–681.

McDonald, B., McAvoy, E.F., Lam, F., Gill, V., de la Motte, C., Savani, R.C., and Kubes, P. (2008). Interaction of CD44 and hyaluronan is the dominant mechanism for neutrophil sequestration in inflamed liver sinusoids. J. Exp. Med. *205*, 915–927.

McDonald, B., Pittman, K., Menezes, G.B., Hirota, S.A., Slaba, I., Waterhouse, C.C., Beck, P.L., Muruve, D.A., and Kubes, P. (2010). Intravascular danger signals guide neutrophils to sites of sterile inflammation. Science *330*, 362–366.

Meakin, P.J., Chowdhry, S., Sharma, R.S., Ashford, F.B., Walsh, S.V., McCrimmon, R.J., Dinkova-Kostova, A.T., Dillon, J.F., Hayes, J.D., and Ashford, M.L. (2014). Susceptibility of Nrf2-null mice to steatohepatitis and cirrhosis upon consumption of a high-fat diet is associated with oxidative stress, perturbation of the unfolded protein response, and disturbance in the expression of metabolic enzymes but not with insulin resistance. Mol. Cell. Biol. *34*, 3305–3320.

Miyao, M., Kotani, H., Ishida, T., Kawai, C., Manabe, S., Abiru, H., and Tamaki, K. (2015). Pivotal role of liver sinusoidal endothelial cells in NAFLD/NASH progression. Lab. Invest. *95*, 1130–1144.

Morinaga, H., Mayoral, R., Heinrichsdorff, J., Osborn, O., Franck, N., Hah, N., Walenta, E., Bandyopadhyay, G., Pessentheiner, A.R., Chi, T.J., et al. (2015). Characterization of distinct subpopulations of hepatic macrophages in HFD/obese mice. Diabetes *64*, 1120–1130.

Obstfeld, A.E., Sugaru, E., Thearle, M., Francisco, A.M., Gayet, C., Ginsberg, H.N., Ables, E.V., and Ferrante, A.W., Jr. (2010). C-C chemokine receptor 2 (CCR2) regulates the hepatic recruitment of myeloid cells that promote obesity-induced hepatic steatosis. Diabetes *59*, 916–925.

Oh, D.Y., Morinaga, H., Talukdar, S., Bae, E.J., and Olefsky, J.M. (2012). Increased macrophage migration into adipose tissue in obese mice. Diabetes *61*, 346–354.

Olefsky, J.M., and Glass, C.K. (2010). Macrophages, inflammation, and insulin resistance. Annu. Rev. Physiol. *72*, 219–246.

Osborn, O., and Olefsky, J.M. (2012). The cellular and signaling networks linking the immune system and metabolism in disease. Nat. Med. *18*, 363–374.

Pajvani, U.B., Shawber, C.J., Samuel, V.T., Birkenfeld, A.L., Shulman, G.I., Kitajewski, J., and Accili, D. (2011). Inhibition of Notch signaling ameliorates insulin resistance in a FoxO1-dependent manner. Nat. Med. *17*, 961–967.

Park, H.W., Park, H., Ro, S.H., Jang, I., Semple, I.A., Kim, D.N., Kim, M., Nam, M., Zhang, D., Yin, L., and Lee, J.H. (2014). Hepatoprotective role of Sestrin2 against chronic ER stress. Nat. Commun. *5*, 4233.

Petit, A., Bihel, F., Alvès da Costa, C., Pourquié, O., Checler, F., and Kraus, J.L. (2001). New protease inhibitors prevent gamma-secretase-mediated production of Abeta40/42 without affecting Notch cleavage. Nat. Cell Biol. *3*, 507–511.

Rafii, S., Butler, J.M., and Ding, B.S. (2016). Angiocrine functions of organ-specific endothelial cells. Nature *529*, 316–325.

Rockey, D.C., Bell, P.D., and Hill, J.A. (2015). Fibrosis—a common pathway to organ injury and failure. N. Engl. J. Med. *372*, 1138–1149.

Scheibye-Knudsen, M., Fang, E.F., Croteau, D.L., and Bohr, V.A. (2014). Contribution of defective mitophagy to the neurodegeneration in DNA repair-deficient disorders. Autophagy *10*, 1468–1469.

Shetty, S., Weston, C.J., Adams, D.H., and Lalor, P.F. (2014). A flow adhesion assay to study leucocyte recruitment to human hepatic sinusoidal endothelium under conditions of shear stress. J. Vis. Exp. *85*, 1–7.

Talukdar, S., Oh, D.Y., Bandyopadhyay, G., Li, D., Xu, J., McNelis, J., Lu, M., Li, P., Yan, Q., Zhu, Y., et al. (2012). Neutrophils mediate insulin resistance in mice fed a high-fat diet through secreted elastase. Nat. Med. *18*, 1407–1412.

Volpes, R., van den Oord, J.J., and Desmet, V.J. (1990). Hepatic expression of intercellular adhesion molecule-1 (ICAM-1) in viral hepatitis B. Hepatology *12*, 148–154.

Wang, H., Luo, W., Wang, J., Guo, C., Wang, X., Wolffe, S.L., Bodary, P.F., and Eitzman, D.T. (2012). Obesity-induced endothelial dysfunction is prevented by deficiency of P-selectin glycoprotein ligand-1. Diabetes *61*, 3219–3227.